08

Electron Transport in Carbon-Based Nanocomposites for Memristor Nanosystems

© *A.S. Vedeneev, A.M. Kozlov, D.V. Kolodko, V.A. Luzanov*¶, *I.A. Sorokin*

Kotelnikov Radio-Engineering and Electronics Institute
of the Russian Academy of Sciences,
Fryazino, Russia

¶ E-mail: Valery@Luzanov.ru

Received 24 October, 2023
Revised 24 October, 2023
Accepted 24 November, 2023

A technology has been developed for the synthesis of non-doped diamond-like carbon (DLC) and metal-containing carbon nanocomposites based on DLC doped with metal (Cu, Ni, Ti, Mo, W, Fe) for the manufacture of memristor memory elements. The structure of DLC and the features of electron transport in Pt|DLC|Pt and Pt|DLC : Ni|Pt systems with Ni content up to 40 at.% have been studied, and the percolation threshold has been determined. The nature and mechanisms of the nonlinearity of the current–voltage characteristics of the studied structures and further prospects for their application in memristor nanosystems are discussed.

Keywords: diamond-like carbon, physicochemical synthesis, electromigration, hybridization, percolation, resistive switching, spin-relative transport, beam plasma.

DOI: 10.61011/PSS.2024.01.57862.239

1. Introduction

The study of the resistive switching (RS) effects in metal–insulator–metal (MIM) structures is currently of great interest because of prospects for their use in the production of multilevel memory elements and memristor arrays, which emulate synapses in neuromorphic computing devices for the language recognition, decision making, and forecasting [1–6]. Over the past ten years, various materials showing the RS effect have been found and classified according to the mechanism of this effect [1–3].

Effects of RS between the high-resistive state (HRS) and low-resistive state (LRS) of MIM structures are usually associated with electromigration of oxygen vacancies in a dielectric oxide layer (TiO_x, TaO_x, HfO_x, *etc.*) [1–6] accompanied by redox reactions, or electromigration of metal cations such as Cu and Ag in a dielectric (*e.g.*, SiO_2) from the MIM structure active electrode [7]. At the same time, RS caused by the electromigration of oxygen vacancies or metal cations is caused by the formation of conductive filaments or conductive bridges in an oxide matrix, respectively. There are also other mechanisms responsible for the RS, *e.g.*, those associated with spin-polarized transport [8], electrochemical reactions [9], and electron drag effects [10]. However, in practice, the greatest attention is given to MIM structures with RS caused by the electromigration of oxygen anions and/or metal cations in the oxide layer [1–7]. Such memristor structures provide a large number of stable (without degradation) reversible RS cycles between HRS and LRS. Note that in the case of anionic (or cationic) transport mechanisms, the RS has a bipolar character, *i.e.*, switching into LRS and HRS occurs at different polarities of the voltage applied to the structure. In this case, the current–voltage $I(V)$ characteristics of the MIM structures, as a rule, are noticeably asymmetric. Meanwhile, in the case of strongly temperature-dependent redox reactions, it is possible to implement monopolar RS [2] with the voltage switching ratio of $V_{LRS}/V_{HRS} \approx 3$ [11,12].

In the case of MIM structures based on diamond-like carbon (DLC), specific RS effects should be expected. Indeed, the ability of carbon to implement various hybridization types of electron shells (planar „graphene“ sp^2-type, spatial „diamond“ sp^3-type, and linear „carbonic“ sp-type) allows the production of materials containing local regions with different properties (sp^3 is a dielectric with high thermal conductivity, sp^2 is a semimetal, *etc.*). Also notice that in MIM structures with isolating layers based on DLC or amorphous hydrogenated carbon (a-C : H), only RS associated with the electromigration of cations (Ti, Cu) was observed [13,14]. Nevertheless, the $I(V)$ characteristics of iron-doped DLC layers [15] exhibit local $sp^3 \rightarrow sp^2$ transformations in fields $> 3 \cdot 10^5$ V/cm, which can initiate switching of the structure from the HRS to the LRS. Note also that these and other available data indicate a composite character of the DLC layers; *i.e.*, they should be considered as an ensemble of low-resistive sp^2 inclusions (nanoclusters) in the dielectric sp^3 matrix, the defectiveness of which depends on the conditions of the layer synthesis [15,16].

The purpose of present work is to study the properties and RS effects in Pt|DLC|Pt structures based on non-doped and Ni-doped DLC layers.

2. MIM structures based on non-doped DLC

Thin (20 nm) DLC layers were deposited on a Pt-coated (100 nm) oxidized Si substrate by high-frequency diode sputtering of a C target by Ar ions with an increased energy of 2 keV [17]. The phase ratio of the sp^2 and sp^3 hybridization types in the DLC layers was controlled by the growth conditions [17]. The crystal structure of the DLC layers was studied by X-ray diffractometry on a DRON-3 modernized two-crystal X-ray diffractometer in the Bragg–Brentano geometry (Burevestnik, St.Petersburg, Russia) at a wavelength of 0.15405 nm. In addition, the structural features of the layers were studied using combined scattering spectroscopy on an EnSpectrRam-MicsM532 spectrometer (EnSpectr, Chernogolovka, Russia) with a laser wavelength of 532 nm. This study showed that the layers are strongly amorphized (the size of coherent scattering regions ≤ 1 nm is commensurate with the size of the unit cells of carbon materials) and contain regions with the sp^2 and sp^3 hybridization type (see [17]). The increase in the energy of Ar ions caused the increase in the resistance of the structures (from several ohms to > 10 MΩ) because of increase in dielectric phase fraction with the sp^3 hybridization, in our opinion.

2.1. Non-ohmic conductance of high-resistance DLC

It was shown in [18] that the effect of an electric field on the transport of charge carriers by the level of percolation under fluctuation potential (FP) conditions is reduced to a decrease in the activation energy, which can be interpreted as a decrease in the percolation threshold, which does not depend on the average free path of charge carriers. The dependence of the current I on voltage in this case is determined by formula:

$$I \propto \exp[(CeaV_0^{\nu})^{1/(1+\nu)}/k_BT], \quad (1)$$

provided that inequality

$$eEa \gg k_BT(k_BT/V_0)^{\nu} \quad (2)$$

is fulfilled. Here, $E = V/d$ is the electric field strength, d is the thickness of the insulating DLC layer, V_0 is the FP amplitude, a is its characteristic spatial scale, ν is the critical index of the percolation theory (in the 3D case, $\nu \approx 0.9$), $C \approx 0.25$ is the numerical coefficient, e is the electron charge, k_B is the Boltzmann constant, and T is the temperature. Neglecting the difference of index ν from unity, we obtain from (1) [18]:

$$I \propto \exp(\alpha E^{1/2}/k_BT), \quad (3)$$

where $\alpha = (CeaV_0)^{1/2}$, *i.e.*, we have a law similar to the Frenkel–Poole law [19] in which quantity α appears instead of coefficient

$$\beta = 2(e^3/\kappa)^{1/2}, \quad (4)$$

where κ is the dielectric constant of the DLC.

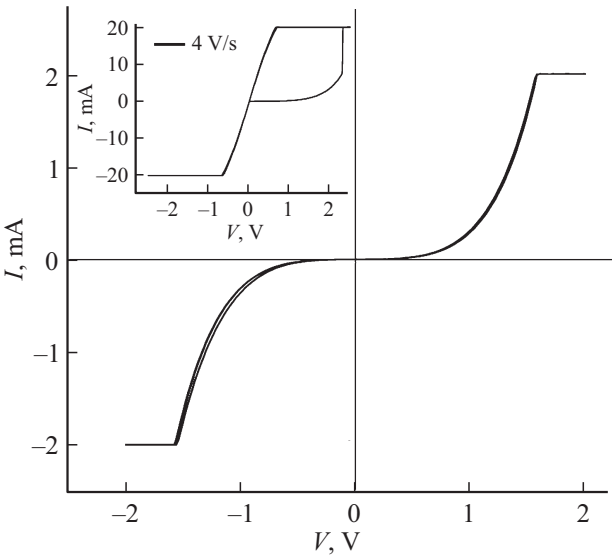

Figure 1. Typical $I(V)$ of a Pt|DLC|Pt structure at the voltage sweep rate of 2 and 4 V/s (the graphs coincide) with a current limitation at the level of 2 mA; the inset shows the structure $I(V)$ in the mode of resistive switching to a low-resistance state that is obtained with a current limitation of $I_c = 20$ mA.

The $I(V)$ characteristics and RS effects were studied at room temperature using a NI PXI-4140 multifunctional source-meter and a PM5 (Cascade Microtech, Beaverton, USA) analytical probe station equipped with a PSM-100 (Motic, Beaverton, USA) specialized system with an optical microscope, which allows micrometric movement of probes (the size of the probe is 5 μm, the movement accuracy is 3 μm) (see details in [20]). The $I(V)$ were studied at room temperature in the current limiting mode at the grounded lower electrode of the structures and the sweep of bias voltage to a linear step law in sequence $0 \rightarrow +3\,\text{V} \rightarrow 0 \rightarrow -3\,\text{V} \rightarrow 0$ with a step amplitude of 0.02 V and its various duration of 5 and 10 ms, which corresponds to the sweep rates of 4 and 2 V/s.

Fig. 1 shows typical dependences of the current I on voltage V for a Pt|DLC|Pt structure that are obtained in the mode of current limit $I_c = 2$ mA and various sweep rates in the voltage range of $|V| < 2$ V. The $I(V)$ are independent of direction and speed of voltage sweep, which indicates their stationary nature. An increase in I_c to 20 mA and $|V| > 2$ V leads to the RS of the structure in a low-resistance state (see the inset to Fig. 1), which can persist for a long time (up to a day). Below, we will consider a possible mechanism of charge carrier transport in the high-resistance state of the structure.

Fig. 2 shows the dependence of structure normalized conductance $G = I/V$ on voltage V in coordinates of $\ln(G/G_0)$ *vs* $V^{1/2}$, which is linear and has a pronounced threshold character; G_0 is the structure conductance in the weak electron field limit. Observed $I(V)$ peculiarities agree with the conclusions of [18].

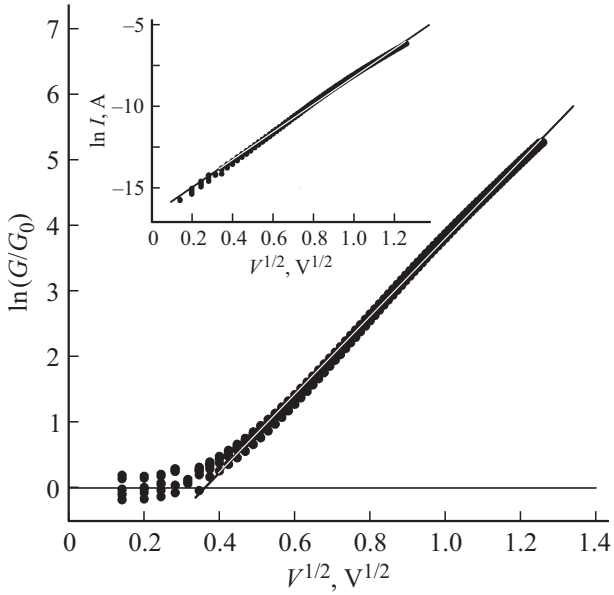

Figure 2. Dependence of conductance G of a Pt|DLC|Pt structure on voltage V. The inset shows the structure $I(V)$ as the function of $\ln(I)$ on the $V^{1/2}$; G_0 is the structure conductance in the weak electron field limit.

Estimate now the characteristic size a of „graphite“ sp^2 nanoclusters. The discontinuity of the conduction band of diamond at the boundary with graphite should be determined by the difference between the graphite work function of $W \approx 4.7$ eV and the electron affinity energies in diamond, the value of which is sufficiently small (~ 0.1 eV) and may even be negative [21]. Since the diamond band gap of $E_g \approx 5.5$ eV [21] slightly exceeds the work function of graphite, the smallest barriers under these conditions are realized for hole transport. In this case, neglecting the effects of size quantization, the characteristic depth of potential wells (FP amplitude) for holes is $V_0 \approx (E_g - W) \approx 0.8$ eV. By the slope of experimental characteristics shown in Fig. 2, we obtain $a \approx 4$ nm, which seems to be a reasonable value [17].

Thus, the non-linear behavior of the conductivity of Pt|DLC|Pt structures in the HRS mode is due to field effects under conditions of percolation transport of charge carriers in the fluctuation potential initiated by fluctuations in the composition of DLC layers in the presence of low-resistance sp^2 nanoclusters in a diamond-like sp^3 matrix. The characteristic size of sp^2 nanoclusters estimated within the framework of the percolation model as ~ 4 nm agrees with the results of X-ray diffraction analysis of DLC films [17].

2.2. Monopolar resistive switching effect

The $I(V)$ characteristics of the non-doped DLC MIM structures were studied at room temperature in the „vertical“ geometry. Platinum electrodes were chosen because Pt does not produce mobile ions in the DLC, thus the studied RS effects should not be associated with the electromigration of ions. The bias voltage V in a range of 0−30 V was applied through a limiting resistor R_L on a Pt probe pressed to the DLC surface. The $I(V)$ characteristic was measured at the variation of V with a rate of ~ 0.1 V/s.

Fig. 3 illustrates the dependence of the current I on the voltage drop V on the structure measured at $R_L = 100$ kΩ. Initially, the structures were in the high-resistive state with the resistance $R = V/I \approx 120$ kΩ. With increasing voltage, the resistance of the structures drops to ~ 10 kω, and at $V \geq 3$ V, the structures are switched in ~ 100 s to the LRS with $R \approx 2-3$ kΩ. The LRS persists with decreasing V and the structure is switched to the HRS with $R \approx 100$ kΩ at $V \geq 0.1$ V in ~ 300 s. At the negative voltage polarity, the structure exhibits similar behavior, which is quite clearly manifested when the inverted $I(V)$ characteristic obtained at negative bias is compared to the $I(V)$ characteristic measured at $V > 0$, which is shown in Fig. 4. Fig. 4 shows that both $I(V)$ branches for $V > 0$ and $V < 0$ coincide

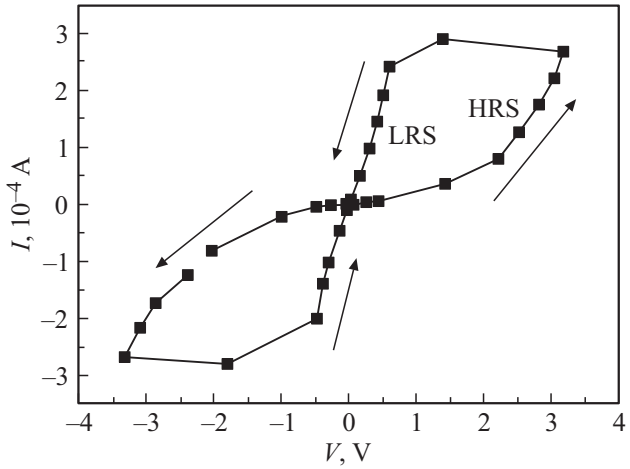

Figure 3. The $I(V)$ of the Pt|DLC|Pt structure. The arrows indicate the measurement sequence.

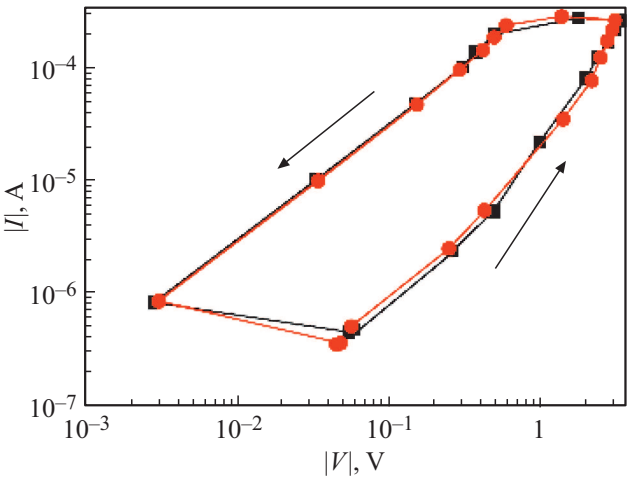

Figure 4. Log–log plots of $|I|$ vs $|V|$ for positive (circles) and negative (squares) voltage polarity.

within 10%. To the best of our knowledge, such a hysteresis behavior of the $I(V)$ characteristics in MIM structures with ion transport was not observed previously.

It is remarkable that the dependences of $\log|I|$ on $\log|V|$ for the HRS in Fig. 4 demonstrate several linear sections with different exponents $n(I \propto V^n)$: linear Ohm's law with $n \approx 1.1$ at $V \geq 0.4\,\mathrm{V}$, then a power law with $n \approx 1.6$ in a range of $0.5\,\mathrm{V} \leq V \leq 2\,\mathrm{V}$, and an exponential law with $n \approx 3.3$ at $V \geq 2\,\mathrm{V}$. The exponential law with $n \approx 2$ is often associated with the appearance of space-charge limited currents [22], which in the presence of traps can be replaced by the region of the sharp current growth ($n \geq 3$) under the conditions of their maximum filling [12,13,23]. Within the concept of space-charge limited currents, it is possible to obtain estimates characterizing the structures under study in this mode.

Taking into account that the transition from the ohmic to the exponential-law region with $n \approx 2$ in the $I(V)$ characteristic occurs when the density of the charge injected into the DLC, $n_i \approx \kappa V/2\pi e d^2$ (here, $\kappa \approx 6$ [16], $d \approx 20\,\mathrm{nm}$), exceeds the equilibrium charge-carrier density [22], from the voltage of this transition $V \approx 0.3\,\mathrm{V}$ (Fig. 4), we find $n_i \sim 10^{18}\,\mathrm{cm}^{-3}$. Such a high equilibrium charge-carrier density at the structure resistance of $\sim 100\,\mathrm{k\Omega}$ means that the electron transfer in the DLC layer in the HRS occurs most likely through electron hopping between sp^2 nanoclusters.

Note that the non-linearity of $I(V)$ characteristics under hopping transport conditions may have a different nature. The transverse hopping conductivity of thin films is substantially determined by mesoscopic effects such as the formation of percolation chains formed by centers with the narrowest center-to-center (in our case, intercluster) potential barriers [24,25], in which the maximum electric field is reached. Electron transfer at the percolation conductivity in the non-ohmic mode was considered in [18], where it was shown that transition to the exponential dependence occurs in relatively strong fields $eE > k_\mathrm{B}T(k_\mathrm{B}T/V_0)^\nu$. At the same time, the $I(V)$ characteristic takes a form similar to the Frenkel–Poole law: $I \propto \exp(\alpha E^{1/2}/k_\mathrm{B}T)$, where $\alpha = (CeaV_0)^{1/2}$ where $C \approx 0.3$ [26], and V_0 and a are the amplitude and characteristic spatial scale of potential fluctuations, respectively.

In our case, it is natural to associate the fluctuation potential with the chaotic distribution of the charge localized on electrically active defects in the DLC matrix. The experimental dependence of $\log I$ on $V^{1/2}$ (Fig. 5) demonstrates a linear region in the range of $1\,\mathrm{V} \leq V \leq 3\,\mathrm{V}$, which slope gives $\alpha(\partial E/\partial V)^{1/2}/k_\mathrm{B}T \approx 2.6\,\mathrm{V}^{-1/2}$. Under the assumption that $\partial E/\partial V \approx 1/d$, the above expressions give the estimation of $aV_0/d \approx [\partial \ln I/(\partial V^{1/2})]^2(k_\mathrm{B}T)^2/Ce^2 \approx 14\,\mathrm{meV}$ and the percolation cluster correlation radius $L_0 \approx a(V_0/k_\mathrm{B}T) \approx 12\,\mathrm{nm}$, which implies that $L_0/d \approx 1$. Therefore, the systems under study should be considered mesoscopic, where hopping transfer occurs mainly through single chains of sp^2 nanoclusters, and both the electric field and the local current density are sharply increased.

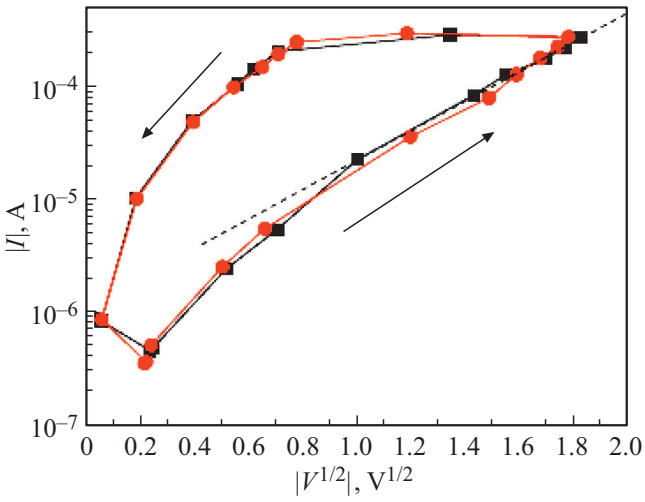

Figure 5. Log–log plots of $|I|$ *vs* $|V|^{1/2}$ for positive (circles) and negative (squares) voltage polarity.

Note that in the LRS case, the current depends linearly on the voltage (Fig. 4), which contradicts the classical concepts of space-charge limited currents, within which $I \propto V^2$ [22]. Previously, this behavior was found in Ti|DLC|Pt structures [13], which implies RS mechanisms related to the formation of conductive bridges owing to the electromigration of Ti cations under the conditions of space-charge limited currents [13].

In our structures, both electrodes are made of inert metal (Pt); therefore this mechanism is hardly essential. In addition, under the conditions of cations electromigration, the $I(V)$ characteristics are noticeably asymmetric [13], whereas the situation in our case is opposite (Fig. 5).

It was noted in [15] that the strong fields of $\geq 3 \cdot 10^5\,\mathrm{V/cm}$ stimulate the change in the hybridization type of the diamond-like sp^3 DLC regions, which separate the conducting sp^2 regions (nanoclusters). This process is accompanied by the growth/overlap of sp^2 clusters and the structure transition from the HRS to the LRS. Meanwhile, in weak fields, reverse $sp^2 \rightarrow sp^3$ transformations prevail, causing the reverse RS. Since HRS $\rightarrow$ LRS switching is observed in fields of $\sim 10^6\,\mathrm{V/cm}$, and reverse switching occurs in zero fields (Fig. 3), we conclude that the noted mechanism is responsible for the effects of reversible resistive switching in the studied structures.

Thus, the $I(V)$ features observed in the HRS are caused by field effects under the conditions of percolation charge carrier hopping between low-resistive sp^2 nanoclusters separated by diamond-like sp^3 gaps. The change of the hybridization type in sp^3 gaps initiates switching in a strong electric field (*i. e.*, in the strong non-equilibrium situation), which is observed as the effect of limiting trap filling. At the same time, in the equilibrium situation (in a weak field), the reverse $sp^2 \rightarrow sp^3$ transitions prevail, which transforms the structure to the HRS.

3. DLC with Ni impurity

The addition of different element atoms changes the DLC film properties. Impurities of F, N, Cu, Ti, Ta, W, Nb, Ag, Co, or Si affect the friction factor, hardness, optical properties, and film conductivity [27–37]. Dielectric properties of the DLC films with the Ni impurity were studied in [37–39]. Mechanisms of non-doped DLC film conductance non-linear behavior we have studied earlier [40–42]. It was noted that this behavior may be caused by the effects of Frenkel–Poole [19], Shottky [43], resistive switching due to cation electro-migration or changing the carbon hybridization type in a strong electric field [13,14,44], charge carrier percolation in random Coulomb potential [18,45], *etc.* In the case of hopping electron transport, the $I(V)$ non- linearity could be also caused by mesoscopic effects, *i.e.*, by the formation of percolation chains of centers separated by most narrow potential barriers [24,27], where most strong electric field occurs.

Thin (40 nm) DLC(Ni) films were synthesized in discharge with hollow Ni cathode in the mixture of argon and propane at the simultaneous deposition of the DLC and Ni. The DLC(Ni) films were grown in the plasma-chemical reactor (PCR) [46]. The electrode system of the PCR contains the cathode shaped as a hollow cylinder with a diameter of 18 mm, a length of 35 mm, and a thickness of 1 mm; the vacuum chamber frame was used as the anode. The 2-mm-thick glass plate covered with Pt film (bottom electrode) was used as the substrate. The Ni concentration (of 10, 20, and 40 at.%) was set by variation of the portion of propane (reactive gas) in the plasma-creative gas (argon) in the frames of $C_3H_8:Ar \approx 1:(1000-7000)$. The rate of the DLC(Ni) film deposition and Ni content for different portions of propane in argon is shown in Fig. 6.

The crystalline structure of the DLC(Ni) films was studied by the method of [17]. It was shown that the typical size of the Ni inclusions (nanoclusters) does not exceed 0.5 nm which is in agreement with the results of [39].

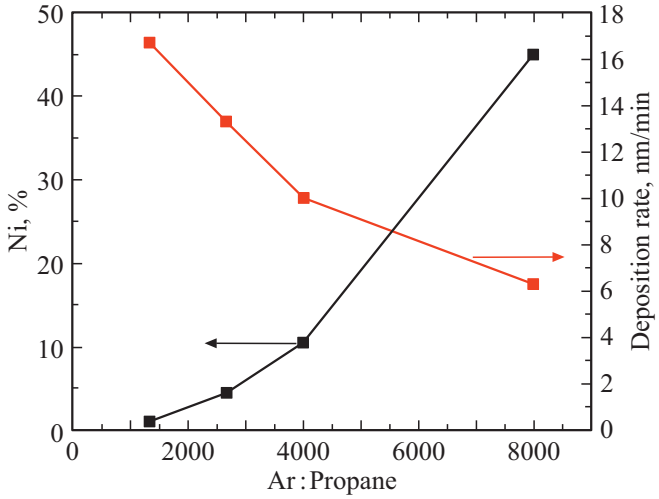

Figure 6. The dependence of Ni content and the rate of the DLC(Ni) film deposition on argon to propane ratio.

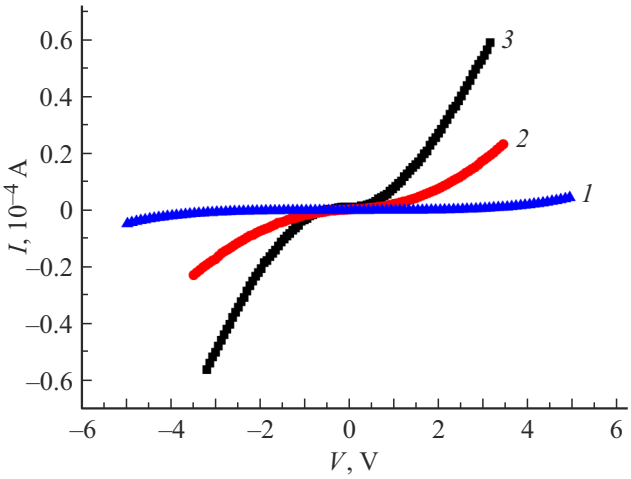

Figure 7. Typical $I(V)$ of the Pt|DLC(Ni)|Pt structure with different Ni content: curve *1* — 10, *2* — 20, *3* — 40 at.%.

3.1. Non-linearity of $I(V)$ characteristics

At $I(V)$ measurements, the Pt sub-layer was used as the bottom electrode, and the clipping Pt probe was used as the top electrode. The voltage with the amplitude of $V_a = 5$ V was set by the generator Tektronix AFG 3252 (Tektronix, Portland, USA), and the current and the voltage drop on the film were measured by the digital oscillograph Tektronix TPS 2024. The current value was calculated by the voltage drop on the standard resistor of 10 kΩ. Fig. 7 illustrates typical room temperature $I(V)$ of the Pt|DLC(Ni)|Pt structure with the Ni content of 10, 20, and 40 at.%.

The $I(V)$ are of the non-linear type which is typical for the DLC-based structures (see [40–42]). The voltage increase for $|V| > V_a$ leads to the structure switching from the high-resistive to the low-resistive state, which keeps itself for a long time.

Because of the small size of the Ni inclusions, we assume that $I(V)$ non-linearity could be associated with the Frenkel–Poole effect, for which the structure conductance G depends on the electric field $E \propto V$ as $G \propto \ln(AE^{1/2})$, where $A = 2(e^3/\kappa)^{1/2}/k_B T$. Indeed, the dependences of the G on V could be linearized in the scale of $\ln(G)\, vs\, V^{1/2}$ (see Fig. 8).

As follows from the data of Fig. 8, the structure conductance increases with the Ni content, while the slope of the $\ln(G)\, vs\, V^{1/2}$ curves decreases, which contradicts the Frenkel–Poole effect. Indeed, the coefficient A in this model does not depend on the Ni content. The reason for this contradiction could be associated with the increase of the DLC(Ni) dielectric constant with the Ni concentration increase (see [39]).

Note that one of the composite system's main characteristics is the percolation threshold, *i.e.*, the metal concentration

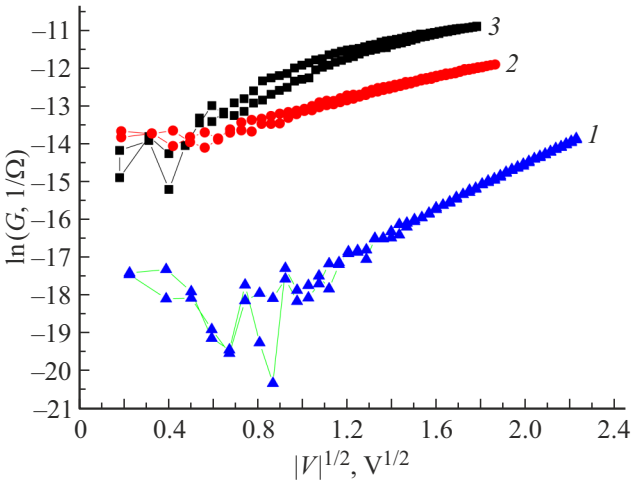

Figure 8. Dependence of the DLC(Ni) conductance G on $|V|^{1/2}$ at different Ni content: curve *1* — 10, *2* — 20, *3* — 40 at.%.

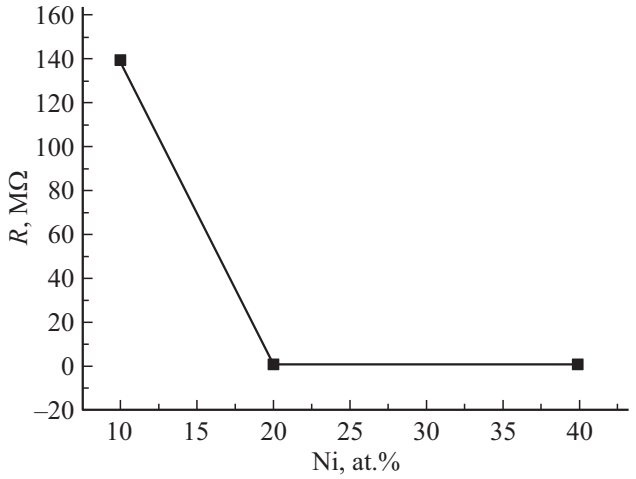

Figure 9. The dependence of the Pt|DLC(Ni)|Pt structure resistance R on the Ni content.

at which the infinite conducting cluster occurs [45]. Fig. 9 illustrates the dependence of the Pt|DLC(Ni)|Pt structure resistance $R = 1/G$ on the Ni content. The percolation threshold corresponds to the Ni concentration of ~ 20 at.% in correspondence with the results of [39].

4. Conclusions

A technology has been developed for the synthesis of non-doped diamond-like carbon (DLC) and metal-containing carbon nanocomposites based on Ni-doped DLC for the manufacture of memristive memory elements. The Pt|DLC|Pt structures are fabricated by high-frequency diode sputtering of a C target by Ar ions, or in discharge with hollow Ni cathode in the mixture of argon and propane at the simultaneous deposition of the DLC and Ni.

As shown, in our case the nonlinear behavior of the conductivity of Pt|DLC|Pt structures based on non-doped DLC in the HRS mode is due to (i) field effects under conditions of percolation transport of charge carriers in the fluctuation potential initiated by fluctuations in the composition of DLC layers in the presence of low-resistance sp^2 nanoclusters in a diamond-like sp^3 matrix, or (ii) by the change of the hybridization type in sp^3 gaps in a strong electric field. The characteristic size of sp^2 nanoclusters estimated within the framework of the percolation model of ~ 4 nm agrees with the results of X-ray diffraction analysis of DLC films. Non-linear $I(V)$ of Pt|DLC(Ni)|Pt structures with the Ni concentration of 10, 20, and 40 at.% are in agreement with the Frenkel–Poole model. The increase of the Ni content leads to an increase of the structure conductance G, while the slope of the $\ln(G)$ *vs* $V^{1/2}$ curves decreases. The reason for this contradiction could be associated with an increase of the DLC(Ni) dielectric constant with the Ni concentration increase. The percolation threshold corresponds to the Ni concentration of ~ 20 at.% in correspondence with known results.

Funding

The reported study was funded by Russian Science Foundation, grant No. 23-29-00276 „Memristor systems based on diamond-like carbon: synthesis, electron transport, and effects of resistance switching“.

References

[1] J.S. Lee, S. Lee, T.W. Noh. Appl. Phys. Rev. **2**, *3*, 031303 (2015).
[2] Resistive switching: from fundamentals of nanoionic redox processes to memristive device applications / Eds D. Ielmini, R. Waser. John Wiley & Sons (2015).
[3] D. Ielmini. Semicond. Sci. Technol. **31**, *6*, 063002 (2016).
[4] D.H. Kwon, K.M. Kim, J.H. Jang, J.M. Jeon, M.H. Lee, G.H. Kim, X.-S. Li, G.-S. Park, B. Lee, S. Han, M. Kim, C.S. Hwang. Nature Nanotechnol. **5**, *2*, 148 (2010).
[5] M. Kyu Yang, H. Ju, G. Hwan Kim, J.-K. Lee, H.-C. Ryu. Sci. Reps. **5**, *1*, 14053 (2015).
[6] H. Jiang, L. Han, P. Lin, Z. Wang, M.H. Jang, Q. Wu, M. Barnell, J.J. Yang, H.L. Xin, Q. Xia. Sci. Reps **6**, *1*, 28525 (2016).
[7] A. Mehonic, A.L. Shluger, D. Gao, I. Valov, E. Miranda, D. Ielmini, A. Bricalli, E. Ambrosi, C. Li, J.J. Yang, Q. Xia, A.J. Kenyon. Adv. Mater. **30**, *43*, 1801187 (2018).
[8] J. Grollier, D. Querlioz, M.D. Stiles. Proceed. IEEE **104**, *10*, 2024 (2016).
[9] D.A. Lapkin, A.V. Emelyanov, V.A. Demin, V.V. Erokhin, L.A. Feigin, P.K. Kashkarov, M.V. Kovalchuk. Appl. Phys. Lett. **112**, *4*, 043302 (2018).
[10] A.S. Vedeneev, V.V. Rylkov, K.S. Napolskii, A.P. Leontiev, A.A. Klimenko, A.M. Kozlov, V.A. Luzanov, S.N. Nikolaev, M.P. Temiryazeva, A.S. Bugaev. JETP Lett. **106**, *6*, 411 (2017).
[11] U. Russo, D. Ielmini, C. Cagli, A.L. Lacaita. IEEE Trans. Electron. Devices **56**, *2*, 186 (2009).

[12] Y. Sharma, P. Misra, R.S. Katiyar. Appl. Phys. Lett. **116**, *8*, 084505 (2014).
[13] P. Peng, D. Xie, Y. Yang, Y. Zang, X. Gao, C. Zhou, T. Feng, H. Tian, T. Ren, X. Zhang. J. Appl. Phys. **111**, *8*, 084501 (2012).
[14] F. Zhuge, W. Dai, C.L. He, A.Y. Wang, Y.W. Liu, M. Li, Y.H. Wu, P. Cui, R.-W. Li. Appl. Phys. Lett. **96**, *16*, 163505 (2010).
[15] X. Liao, X. Zhang, K. Takai, T. Enoki. J. Appl. Phys. **107**, *1*, 013709 (2010).
[16] S. Takabayashi, M. Yang, S. Ogawa, H. Hayashi, R. Ješko, T. Otsuji, Y. Takakuwa. J. Appl. Phys. **116**, *9*, 093507 (2014).
[17] V.A. Luzanov, A.S. Vedeneev. J. Commun. Technol. Electron. **63**, *9*, 1068 (2018).
[18] B.I. Shklovskii. Sov. Phys. Semicond.-USSR **13**, *1*, 53 (1979).
[19] J. Frenkel. Phys. Rev. **54**, *8*, 647 (1938).
[20] V.A. Levanov, A.V. Emel'yanov, V.A. Demin, K.E. Nikirui, A.V. Sitnikov, S.N. Nikolaev, A.S. Vedeneev, Yu.E. Kalinin, V.V. Ryl'kov. J. Commun. Technol. Electron. **63**, *5*, 491 (2018).
[21] N. Eimori, Y. Mori, A. Hatta, T.I.T. Ito, A.H.A. Hiraki. Jpn. J. Appl. Phys. **33**, *11R*, 6312 (1994).
[22] M.A. Lampert, R.B. Schilling. In: Semiconductors. Semimetals **6**, 1–96, Elsevier (1970).
[23] N. Andreeva, A. Ivanov, A. Petrov. AIP Advances **8**, *2*, 025208 (2018).
[24] M. Pollak, J.J. Hauser. Phys. Rev. Lett. **31**, *21*, 1304 (1973).
[25] M.É. Raĭkh, I.M. Ruzin. Soviet JETP Lett. **43**, *9*, 562 (1986).
[26] B.A. Aronzon, D.Y. Kovalev, V.V. Ryl'kov. Semiconductors **39**, *7*, 811 (2005).
[27] A. Khurshudov, K. Kato, S. Daisuke. J. Vacuum Sci. Technol. A **14**, *5*, 2935 (1996).
[28] Q. Wei, R.J. Narayan, A.K. Sharma, J. Sankar, J. Narayan. J. Vacuum Sci. Technol. A **17**, *6*, 3406 (1999).
[29] H. Dimigen, C.-P. Klages. Surface. Coatings Technol. **49**, 1–3, 543 (1991).
[30] X.M. He, M. Hakovirta, M. Nastasi. Mater. Lett. **59**, *11*, 1417 (2005).
[31] J.C. Damasceno, S.S. Camargo Jr, F.L. Freire Jr., R. Carius. Surface. Coatings Technol. **133**−**134**, 247 (2000).
[32] R. Gampp, P. Gantenbein, Y. Kuster, P.P. Reimann, R. Steiner, P. Oelhafen, S. Brunold, U. Frei, A. Gombert, R. Joerger, W. Graf, M. Koehl. Proceed. Soc. Photo-Opt. Instrum. Eng. **2255**, *1*, 92 (1994).
[33] C. Donnet, J. Fontaine, A. Grill, V. Patel, C. Jahnes, M. Belin. Surface. Coatings Technol. **94**−**95**, 531 (1997).
[34] M. Grischke, K. Bewilogua, K. Trojan, H. Dimigen. Surface. Coatings Technol. **74**−**75**, *2*, 739 (1995).
[35] Q. Wei, J. Sankar, J. Narayan. Surface. Coatings Technol. **146**−**147**, 250 (2001).
[36] L.V. Lutsev, S.V. Yakovlev, V.I. Siklitskii. Phys. Solid State **42**, *6*, 1139 (2000).
[37] L.V. Lutsev, T.K. Zvonareva, V.M. Lebedev. Tech. Phys. Lett. **27**, *8*, 659 (2001).
[38] G.A. Nikolaichuk, S.V. Yakovlev, O.Y. Moroz, E.Y. Nakvasina. In: 13th Int. Conf. on Electromechanics, Electrotechnology, Electromaterials and Components (ICEEE). (2010). V. 4. P. 46−49.
[39] G.A. Nikolaichuk, O.Y. Moroz, S.M. Dunaevskii. Tech. Phys. **63**, *11*, 1620 (2018).
[40] A.S. Vedeneev, V.A. Luzanov, V.V. Rylkov. JETP Lett. **109**, *3*, 171 (2019).
[41] S.N. Nikolaev, A.S. Vedeneev, V.A. Luzanov, A.V. Emel'yanov, A.M. Kozlov, A.S. Bugaev, V.V. Ryl'kov. J. Commun. Technol. Electron. **66**, *10*, 1196 (2021).
[42] A.S. Vedeneev, V.V. Ryl'kov, V.A. Luzanov, S.N. Nikolaev, A.M. Kozlov, A.S. Bugaev. J. Commun. Technol. Electron. **68**, *8*, 920 (2023).
[43] K.A. Nasyrov, V.A. Gritsenko. Phys. — Usp. **56**, *10*, 999 (2013).
[44] S. Takabayashi, M. Yang, S. Ogawa, H. Hayashi, R. Ješko, T. Otsuji, Y. Takakuwa. J. Appl. Phys. **116**, *9*, 093507 (2014).
[45] B.I. Shklovskii, A.L. Efros. Electronic Properties of Doped Semiconductors. Springer Science & Business Media (2013). V. 45.
[46] I.A. Sorokin, D.V. Kolodko, K.I. Krasnobaev. J. Commun. Technol. Electron. **65**, *3*, 286 (2020).